

4 Yue Sun<sup>1</sup>, Chuanfeng Zhao<sup>1</sup>

7 Correspondence to: Chuanfeng Zhao ([czhao@bnu.edu.cn](mailto:czhao@bnu.edu.cn))

1



## 28    **1. Introduction**

29    Aerosols can modify radiative energy balance, cloud physics, and precipitation and then affect both  
30    weather and climate, bringing large uncertainties to weather forecast and climate assessment  
31    (Edenhofer and Seyboth, 2013; Tao et al., 2012). Associated with the rapid economic development in  
32    China, heavy aerosol pollution has also resulted in serious impacts on atmospheric environment,  
33    weather, climate, and even public health (An et al., 2019; Song et al., 2017; Wang et al., 2017).  
34    Although the PM<sub>2.5</sub> mass concentrations have decreased significantly since 2013 due to the major air  
35    pollution control measures made by Chinese government (Ding et al., 2019; Fan et al., 2020; Wang et  
36    al., 2020; Zhang et al., 2020; Zheng et al., 2018), China is still among the regions with high aerosol  
37    amount. Thus, it is still necessary to further investigate the aerosol's impacts in China.

38    The aerosol can affect the cloud and precipitation by changing the radiation directly and by serving as  
39    cloud condensation nuclei (CCN) or ice nuclei (IN), which are referred as radiative effect and  
40    microphysical effect. On one hand, the aerosols can scatter and absorb solar radiation, which can heat  
41    the atmosphere and cool the surface, stabilize the atmosphere, and then suppress precipitation.  
42    Particularly, aerosol by absorbing solar radiation can strengthen the evaporation of cloud and then  
43    suppresses the formation of cloud and precipitation (Ackerman et al., 2000). On the other hand,  
44    aerosols, by serving as CCN or IN, can increase cloud droplet number concentration, resulting in larger  
45    cloud albedo (Twomey, 1977), enhanced cloud thermal emissivity (Garrett and Zhao, 2006; Zhao and  
46    Garrett, 2015), reduced precipitation and longer cloud lifetime (Albrecht, 1989; Pincus and Baker,  
47    1994), and invigorated convective precipitation (Fan et al., 2015; Li et al., 2011; Rosenfeld et al., 2008).

48    The aerosols show distinct influences on precipitation under different climatic regions, which make  
49    humid areas wetter and arid areas drier (Huang et al., 2006a; Huang et al., 2006b; Huang et al., 2010;  
50    Koren et al., 2005; Rosenfeld, 2000; Teller and Levin, 2006; Wang, 2005). Using long-term ground site  
51    observations, Li et al. (2011) have found that the increasing aerosols make the cloud higher and deeper  
52    under humid condition, which can increase the frequency and intensity of precipitation significantly  
53    and then increase the probability of floods; while under dry condition, aerosols can inhibit the  
54    development of cloud and precipitation and then increase the probability of drought. Based on the  
55    global satellite data, Niu and Li (2012) have further found that the above phenomenon is shown not  
56    only at single ground site, but even more pronounced in tropical regions. Considering the complexity of



precipitation processes and their variations with locations, studying the aerosol-precipitation interactions is important to improve the accuracy of regional weather forecasts (Fan et al., 2015). The significant influences of aerosol on cloud and precipitation in China have been reported in many studies. In the southeast China, with the increase of the aerosol, the light and moderate precipitations are inhibited, while the heavy precipitations are enhanced (Shi et al., 2015; Wu et al., 2015; Yang et al., 2018). The aerosols over urban region can increase the total amount of precipitation in the case with sufficient moisture supply and decrease the total precipitation amount in the case with insufficient moisture supply (Chen et al., 2015; Qiu et al., 2017). Yang et al. (2017) found that the aerosols can reduce the precipitation areas and intensity over Beijing-Tianjin-Hebei region using WRF-Chem model simulations. Zhao et al. (2018) indicated that the aerosols can reduce the precipitation intensity while enlarge the precipitation area of tropical cyclones over western pacific area using long-term observations. Most existing studies about the impacts of aerosol on precipitation have focused on the precipitation amount, frequency, and intensity, but few studies have investigated how the aerosols affect precipitation time, including both start and peak time of precipitation. Several studies have pointed out that aerosols can make cloud higher and deeper under polluted condition, which will delay the precipitation and cause strong thunderstorm precipitation in downwind areas (Andreae et al., 2004; Lin et al., 2006; Rosenfeld et al., 2008). However, this effect, called as invigoration effect, has not gained widely recognition. Several model simulation studies have shown that the invigoration effect is weak and the aerosols even suppress convection in case with strong wind shear or with cloud cloud base (Fan et al., 2013; Fan et al., 2012; Fan et al., 2009; Khain et al., 2005; Lebo and Morrison, 2014). Moreover, the delay caused by the invigoration effect has not yet been quantified. The limited studies regarding the influence of aerosol on precipitation time showed controversial findings in China. Yang et al. (2017) found that aerosols show no influence on precipitation time in Beijing-Tianjin-Hebei region using WRF-Chem model simulations, while Zhou et al. (2020) reported that aerosols advance the heavy precipitation start and peak time significantly, and prolong the duration of the precipitation in Beijing-Tianjin-Hebei (BTH) region. Similar researches have been carried out by Guo et al. (2016) and Lee et al. (2016) in Pearl River Delta (PRD) region. Guo et al. (2016) found that the aerosol can delay heavy precipitation, which was further confirmed by model simulations (Lee et al., 2016). Guo et al. (2016) and Lee et al. (2016) found that the aerosol radiative effect is dominant in



87 the initial stage of convection and the microphysical effect is dominant in the development stage, and  
88 the interaction of radiative and microphysical effects eventually delays precipitation.  
89 The controversial findings from limited previous studies raise a serious question: Why do the aerosols  
90 show different impacts on the start and peak time of precipitation over different regions? To answer  
91 this question, this study investigates the impacts of aerosols on the start and peak time of precipitation  
92 over three different regions of North China Plain (NCP), YRD, and PRD by using data from the same  
93 source with the same analysis method. With the support of high-precision data, this study tries to  
94 quantify the impacts of aerosols on precipitation time. The responses of convective and stratiform  
95 precipitation to aerosols are also investigated based on the precipitation type. Moreover, the changes of  
96 aerosol impacts on precipitation time with meteorological conditions that can affect precipitation have  
97 also been investigated, including the relative humidity, low troposphere stability, and vertical wind  
98 shear, which are essential to aerosol-cloud-precipitation interactions (Boucher and Quaas, 2012; Fan et  
99 al., 2009; Klein, 1997; Slingo, 1987; Zhou et al., 2020).  
100 The paper is organized as follows. Section 2 describes the data and methods used in this study. Section  
101 3 shows the analysis and results. The summary and discussion are provided in section 4.

## 102 2. Data and methods

### 103 2.1 Region of Interest

104 Three study regions of NCP, YRD, and PRD have been selected in this study, where the concentration  
105 and types of aerosols are different. The  $PM_{2.5}$  mass concentration decreases gradually from north to  
106 south in China. The mixed-absorbing aerosols are dominant in NCP, which can absorb solar radiation  
107 strongly and then heat atmosphere, followed by urban and industrial aerosols (Chen et al., 2014; He et  
108 al., 2020). The dominant aerosols in the YRD are urban, industrial and mixing-absorbing aerosols (Che  
109 et al., 2018; Chen et al., 2013; Chen et al., 2014; He et al., 2020). The main aerosol types in the PRD  
110 are urban and industrial aerosols (Chen et al., 2014; He et al., 2020). It is worth noting that the  
111 absorbing aerosols increase in North China Plain and Yangtze River Delta in June and August due to  
112 biomass burning (Che et al., 2018; Chen et al., 2014).  
113 Figure 1 shows the study region with surface altitude (m) information from Digital Elevation Model  
114 (DEM), along with the location of  $PM_{2.5}$  ground site stations. Due to the topographic rain effect, this



115 study only selects the area with DEM less than 100 meters as the study region. There are 131, 100, and  
116 70 ground sites in NCP, YRD, and PRD, respectively. In order to obtain enough precipitation samples  
117 and then reduce the statistical error, the selected study period is the summer (June to August) of  
118 multiple years from 2015 to 2020.

## 119 2.2 Data

120 The datasets including precipitation, aerosol, and meteorological fields are used in this study, which  
121 are described as follows.

### 122 2.2.1 Precipitation data from GPM

123 The Global Precipitation Measurement (GPM) mission can provide global observations of rain and  
124 snow. Compared to the Tropical Rainfall Measuring Mission (TRMM), the GPM extends capability to  
125 measure light rain ( $< 0.5$  mm/hr), solid precipitation, and the microphysical properties of precipitating  
126 particles, in addition to the ability of observing heavy to moderate precipitation. The observation  
127 devices are the first space-borne Ku/Ka band Dual-frequency Precipitation Radar (DPR) and a  
128 multi-channel GPM Microwave Imager (GMI). The DPR Level-2A product is used in this study.

129 The DPR instrument can provide three dimensional measurements of precipitation structure over 78  
130 and 152 miles (125 and 245 km) swaths. The combination of detection information from the Ka band  
131 precipitation radar (KaPR) and Ku band precipitation radar (KuPR) can retrieve precipitation particle  
132 size distribution and snowfall events effectively, which is beneficial to facilitate the understanding of  
133 precipitation nature and structure deeply. The DPR Level-2A product with a temporal resolution of 90  
134 minutes provides precipitation profile data from ground to 21,875 meters at 125 meters vertical  
135 intervals, including precipitation position, type, and intensity, the height of freezing level, the height of  
136 storm top, and so on.

137 GPM generally performs better for summer, liquid precipitation, and plain area than for winter, solid  
138 precipitation, and complex terrain area (Chen et al., 2019; Speirs et al., 2017). This study focuses on  
139 the warm season in eastern China and the precipitation is mostly liquid during the study period, so the  
140 DPR Level-2A product is suitable to be used. A major role of the DPR Level-2A product in this study is  
141 to classify the three types of precipitation, which are convective, stratiform, and other.



### 142    **2.2.2 Hourly precipitation from China Merged Precipitation Analysis Version 1.0 product**

143    The other precipitation dataset used in this study is the hourly China Merged Precipitation Analysis  
144    Version 1.0 product. This product has a spatial resolution of  $0.1^\circ$  and a temporal resolution of 1 hr in  
145    China. The hourly precipitation product is downloaded online (<ftp://nwpc.nmc.cn>). The product is  
146    developed based on the observation data at 30,000 automatic stations in China and Climate Prediction  
147    Morphing Technique (CMORPH) data. This product overcomes the shortcoming from ground stations  
148    that is difficult to provide the change of the spatial distribution of the overall climate due to  
149    discontinuous distribution. Simultaneously, this product overcomes the issue of poor accuracy of  
150    satellite products. With these merits, this dataset has been successfully applied to many  
151    precipitation-related studies (Guo et al., 2016; Sun et al., 2019), which provides us the possibility for  
152    examining aerosol impacts on precipitation time in this study.

### 153    **2.2.3 Aerosol data**

154    This study takes use of the hourly  $PM_{2.5}$  mass concentration provided by the China Environmental  
155    Monitoring Station of the national air quality real time release platform with data quality assurance  
156    (<http://beijingair.sinaapp.com>) to represent aerosol. Previous studies have used AOD or  $PM_{10}$  to study  
157    the influence of aerosol on precipitation (Guo et al., 2016; Zhao et al., 2018; Zhou et al., 2020).  
158    However, AOD could be not suitable for many cases since it represents the column-integrated aerosol  
159    amount while precipitation mostly occurs in the troposphere and is more affected by aerosols below  
160    cloud bases.  $PM_{10}$  might be also not suitable for the study of aerosol impacts on precipitation  
161    particularly in case large aerosol particles such as dust exist since  $PM_{10}$  is more representative of large  
162    aerosol particles while cloud condensation nuclei is more related to the aerosol particle number with  
163    sizes larger than 100 nm. Instead,  $PM_{2.5}$  mass concentration is more representative of aerosol particle  
164    amount with sizes larger than 100 nm, so that we choose  $PM_{2.5}$  to represent the aerosol amount in this  
165    study.  
166    The diurnal variation of  $PM_{2.5}$  mass concentration is significant in the study regions, especially over  
167    NCP as shown later. This diurnal variation raises a question for the study of aerosol impacts on  
168    precipitation: what time should we choose for the aerosol observations that have more clear impacts on  
169    precipitation? Figure 2 shows the relationship of  $PM_{2.5}$  mass concentration between the daily mean and  
170    the 7:00-12:00 LT mean, the 13:00-18:00 LT mean, the value in 1 hour before precipitation, the mean



value in 2 hours before precipitation, the mean value in 3 hours before precipitation, the mean value in 4 hours before precipitation, and the mean value in 5 hours before precipitation. As shown, the correlation between daily mean  $\text{PM}_{2.5}$  mass concentration and 7:00-12:00 LT (13:00-18:00 LT) mean  $\text{PM}_{2.5}$  mass concentration is relatively poor ( $r=0.57-0.73$ ) in the three study regions. The correlation coefficients between the daily mean  $\text{PM}_{2.5}$  mass concentration and  $\text{PM}_{2.5}$  mass concentration averaged in 1 (2, 3, 4, 5) hours before precipitation are worse than that between daily mean  $\text{PM}_{2.5}$  mass concentration and 7:00-12:00 LT (13:00-18:00 LT) mean  $\text{PM}_{2.5}$  mass concentration, suggesting that it is not suitable to use  $\text{PM}_{10}$  mass concentration or AOD at a given moment to examine the influence of aerosol on precipitation. Taking into account that the aerosol effect needs time to accumulate, this study selects the 4-hours mean  $\text{PM}_{2.5}$  mass concentration before precipitation to investigate the impact of aerosols on precipitation.

#### 2.2.4 ERA5

As indicated earlier, three essential meteorological variables will be investigated in this study, which are the relative humidity, low troposphere stability, and vertical wind shear. Relative humidity can affect both precipitation process and AOD. And the clouds occurring is closely related to water vapor, for example clear skies were more likely than cloudy skies for relative humidities below 65% (Boucher and Quaas, 2012; Klein, 1997; Slingo, 1980, 1987; Zhou et al., 2020). The low troposphere stability can signify the strength of the inversion that caps the planetary boundary layer, which is correlated with cloud amount (Klein, 1997; Wood and Bretherton, 2006). High LTS generally means a relatively stable atmospheric stratification and low LTS means unstable atmospheric column, which is more favorable for the development of convection (Guo et al., 2016; Klein, 1997; Slingo, 1987). Wind shear implies mechanical turbulence, which can influence detrainment and evaporation of cloud hydrometeors and then affects the aerosol effect on precipitation (Fan et al., 2009; Slingo, 1987; Tao et al., 2007). Fan et al. (2009) found that the vertical wind shear plays a dominant role in regulating aerosol effects on isolated deep convective clouds, which determines whether aerosols suppress or enhance convection. The meteorological datasets including the three key variables shown above are from ERA5 in this study, which is the fifth generation ECMWF (European Centre for Medium-Range Weather Forecasts, ECMWF) reanalysis data (<https://cds.climate.copernicus.eu/>). The ERA5 is better than the ERA-Interim in temporal-spatial resolutions of 1 hour and  $0.25^\circ \times 0.25^\circ$ , respectively, and have



200 contributed to thousands of studies (e.g., Fan et al., 2020; Hoffmann et al., 2019; Urraca et al., 2018;  
 201 Yang et al., 2021). The ERA5 hourly data on pressure levels are used in this study, including  
 202 temperature (at 1000, 975, 950, 925, 900, 875, and 850 hPa), relative humidity (at 850 hPa), vertical  
 203 velocity (at 1000, 975, 950, 925, 900, 875, and 850 hPa) and wind (at 850, and 500hPa) on different  
 204 pressure levels.

### 205 2.3 Methods

206 The hourly precipitation product is shown in grid pattern, but the  $PM_{2.5}$  mass concentration dataset is  
 207 from site observation. Therefore, the matching between precipitation information and  $PM_{2.5}$  mass  
 208 concentration is not point to point. However, the representative area of  $PM_{2.5}$  site observation is  
 209 between 0.25 and 16.25 km<sup>2</sup> (Shi et al., 2018), and the representative area is even larger in clean and  
 210 plain areas, so the vague matching described as follows should be reasonable. Assuming the location of  
 211  $PM_{2.5}$  site is a given point called as A, and the point A is in a certain grid of hourly precipitation product  
 212 that is called as B, the  $PM_{2.5}$  mass concentration at A can then be used to represent the pollution  
 213 condition at B. In order to know the precipitation type at B, we find the nearest location according to  
 214 the latitude and longitude provided by GPM. The ERA5 dataset is also shown in grid pattern and we  
 215 use the same method described above to match hourly precipitation product and the ERA5 dataset.

216 The main method used in this study is cluster analysis. We divide all study period into three groups  
 217 based on the  $PM_{2.5}$  mass concentration, and defined two of them as polluted and clean conditions to  
 218 further investigate the aerosol impacts on precipitation. The detailed method is as follows. First, we sort  
 219 all observations of  $PM_{2.5}$  by removing the abnormal values that are over 2 times the standard deviation  
 220 to get the good quality data group C. Second, we rank the  $PM_{2.5}$  mass concentration observations from  
 221 high to low, and define the top 1/3 of group C as clean condition and the bottom 1/3 group C as  
 222 polluted condition. Similar classification method has been applied to other variables when defining  
 223 their high and low value conditions, such as meteorological conditions including the low troposphere  
 224 stability (LTS), vertical wind shear between 1500 m to 5500 m (WS), and relative humidity (RH). The  
 225 LTS (unit: K) used here is the difference of potential temperature at 700 hPa and 1000 hPa (Slingo,  
 226 1987; Wood and Bretherton, 2006). The relative humidity (unit: %) at 850 hPa is used to represent the  
 227 moisture below the cloud base in this study (Klein, 1997; Zhou et al., 2020). The wind shear (unit: s<sup>-1</sup>)  
 228 can be calculated as (Guo et al., 2016),





$$WS = \frac{\sqrt{(u_{5.5}-u_{1.5})^2+(v_{5.5}-v_{1.5})^2}}{(5500-1500)} \dots\dots\dots (1)$$

where  $u_{5.5}$  and  $u_{1.5}$  are horizontal wind speed at 5500 m and 1500 m, respectively;  $v_{5.5}$  and  $v_{1.5}$  are vertical wind speed at 5500 m and 1500 m, respectively. The wind speed at 1500 (5500) m can be converted to wind speed at 500 (850) hPa by barometric height formula.

### 3. Results

#### 3.1 Characteristics of PM<sub>2.5</sub> and precipitation

Figure 3 shows the diurnal variation of PM<sub>2.5</sub> mass concentration. As shown, the diurnal variation of PM<sub>2.5</sub> mass concentration is strong in NCP and weak in YRD and PRD, which further confirms that the too long time average of PM<sub>2.5</sub> mass concentration cannot reliably represent the aerosol amount that influence the precipitation during a relatively short term. The diurnal variation patterns of PM<sub>2.5</sub> are similar in NCP, YRD, and PRD, with low values in the afternoon and high values at night, along with high PM<sub>2.5</sub> mass concentration values in rush hours. The diurnal variations of PM<sub>2.5</sub> is most likely related to the diurnal variation of boundary layer height (BLH). The high BLH is conducive to the diffusion of pollutants in the afternoon, while the low BLH is not conducive to the diffusion at night. Moreover, the PM<sub>2.5</sub> mass concentration is also high around 12:00 LT in PRD, which is most likely caused by the secondary formation by strong solar radiation.

This study focuses on the start and peak time of precipitation event. We define the precipitation event as a continuous precipitation, that is, no precipitation before and after this precipitation at least for 1 hour. During a precipitation event, the time that precipitation appears is called start time, and the time that precipitation intensity is the highest is called peak time. Figure 4 shows the statistical probability density function (PDF) of precipitation start and peak time. There are more than 800 samples at any given hour in the study regions, make the results statistically convincing. As shown in Figure 4, the precipitation events are more frequent at 14:00-16:00 LT but less frequent at 6:00-8:00 LT, which are corresponding to the time of strong and weak solar radiation, respectively. In general, the cloud droplets occur when the atmosphere gets saturated and the droplets can further become precipitation particles through the processes of condensational growth, collision-coalescence, and so on. Strong solar radiation can increase the atmospheric instability by heating the ground surface, further enhancing the convection and promoting the formation of precipitation. In the following analysis, we set the



continuous periods that over the red dotted line as the period with most frequent occurrence of precipitation (simply called Frequent Period) and we set the periods that below the red dotted line as Infrequent Period. There are subtle differences in the Frequent Periods of the start time (shown in Figure 4a, 4b, and 4c) and peak time (shown in Figure 4d, 4e, and 4f) of precipitation over the same region. Note that we use Frequent (Infrequent) Period (S) and Frequent (Infrequent) period (P) to denote the Frequent (Infrequent) Periods of start time and peak time, respectively.

As shown in Figure 4a-c, the Frequent Periods and Infrequent Periods are different significantly in the three study regions. The Frequent Period (S) is 14:00-21:00 LT in NCP, 11:00-19:00 LT in YRD, and 11:00-18:00 in PRD. The durations of Frequent Period (S) are 8, 9, and 8 hours in NCP, YRD, and PRD, respectively. The initial time of Frequent Period (S) in NCP is three hours later than that in YRD and PRD, likely suggesting that the solar radiation takes longer time to strengthen convection in NCP than in YRD and PRD. In contrast, the Frequent Periods (S) turn into Infrequent Periods (S) soon after sunset in YRD and PRD, while the Frequent Period (S) remains 3 hours after sunset in NCP. This makes the initial time of the Frequent Period (S) different but the durations similar in the three study regions. It is curious why the Frequent Period (S) can remain 3 hours after sunset in NCP and what powers the precipitation or convection during the 3 hours. Figure 3 already shows that the  $PM_{2.5}$  mass concentration is the highest in NCP and the lowest in PRD. In addition, there is a relatively large proportion of aerosols as absorbing type in NCP comparing to that in YRD and PRD (Yang et al., 2016). As known, the aerosol can heat the atmosphere and cool the ground by scattering and absorbing solar radiation. Thus, it is most likely that the large quantities of aerosol particles in NCP weaken the downward surface shortwave radiation in the morning and make the Frequent Period (S) delayed. Simultaneously, the large quantities of aerosol particles could release the heat they absorbed in the low atmosphere to extend the Frequent Period (S) of precipitation after sunset.

The diurnal variation of peak time of precipitation is similar to that of the start time, also with more frequent occurrence in the afternoon and less frequent occurrence in the early morning. As shown in Figure 4d-f, the Frequent Periods (P) are 14:00-21:00, 12:00-20:00, 11:00-19:00 LT in NCP, YRD, and PRD, respectively, which indicates that the peak time is often 1-2 hours later than the start time. In NCP, although the Frequent Period (S) and Frequent Period (P) are the same, the frequency of precipitation peak time at 14:00 LT is lower than that for the precipitation start time, while the frequency at 15:00-16:00 LT is higher than that for the precipitation start time, which further confirms that the peak



time is often 1-2 hours later than the start time.

Figure 5 shows the PDFs of the precipitation duration time and when the peak time occurs after start time. As shown, precipitation events within 2 hours account for more than 50% of all precipitation events, and the precipitation events within 4 hours account for more than 80% of all precipitation events. In fact, long-time precipitation events are mostly related to large-scale weather systems, and the impact of aerosol on them is difficult to identify from the complex meteorological factors. Therefore, the precipitation events selected in this study are those with duration time within 4 hours. As shown in Figure 5d-e, because of the high proportion of short-term precipitation events, the peak time tends to occur shortly after the precipitation start time. More than 90% of the precipitation peak time occur within 4 hours of the precipitation events.

Table 1 shows the sample volume of precipitation events along with the precipitation types obtained from GPM product. There are totally 21,567 matched precipitation events in NCP, with 78.60% (16,951 cases) as stratiform precipitation and 15.59% (3,362 cases) as convective precipitation. The number of other precipitation events is small, so this study does not investigate the other precipitation further. The numbers of precipitation events are 30,659 and 26,861 in YRD and PRD, respectively. The proportions of stratiform precipitation events are higher than 56% both in YRD and PRD, and the proportion of convective precipitation is secondary to the stratiform precipitation with values more than 21%. As shown in Table 1, the proportions of convective precipitation gradually increase and the proportions of stratiform precipitation gradually decrease from NCP, YRD to PRD.

### 3.2 Influence of aerosol on precipitation start (peak) time

We investigate the influence of aerosol on precipitation start and peak time by analyzing their Frequent Period and Infrequent Period, respectively. Figure 6 shows the PDFs of the start and peak time of precipitation events under polluted and clean conditions. During the Frequent Period of precipitation in NCP, the crest of start time is 15:00 LT under polluted condition and 18:00 LT under clean condition, which implies that the start time of precipitation is 3 hours advanced by aerosols. In the Infrequent Period of precipitation start time in NCP, the influences of aerosol on the start time of precipitation are different between before and after sunrise: the start time is 1-2 hours delayed by aerosol after sunrise while there is no significant delay or advance in start time of precipitation by aerosol before sunrise. The diurnal variations of precipitation start time are similar in pattern between polluted and clean



316 conditions in YRD, suggesting that aerosols have no significant impact on the precipitation start time  
317 over YRD. In addition, the crest of precipitation start time during the Frequent Period is about 16:00 LT  
318 under both clean and polluted in YRD. Figure 4 already shows that the crest of precipitation start time  
319 is at 14:00 LT in PRD. Figure 6c further shows that the crest of precipitation start time is at 13:00 LT  
320 under clean condition and at 15:00 LT under polluted condition in PRD during the Frequent Period of  
321 precipitation, while there are no obvious differences in the PDFs of precipitation start time between  
322 polluted and clean conditions during the Infrequent Period.

323 Above results shown in Figure 6 clearly suggest that the influences of aerosol on the start time of  
324 precipitation are distinct over the three study regions, especially during their Frequent Period. The  
325 aerosol can advance, delay, or show almost no effect on the crest of the start time over the NCP, PRD,  
326 and YRD, respectively. Moreover, the aerosols make precipitation more focused in the afternoon and  
327 suppress the precipitation at night over all three study regions, which is most obvious over PRD. The  
328 diurnal variations of the precipitation start time are much more different between the polluted and clean  
329 conditions in PRD. During the period 12:00-22:00 LT, the frequency of precipitation under polluted  
330 condition is higher than that under clean condition, while during the other period contrary phenomenon  
331 is found in PRD.

332 We also investigate the influence of aerosol on the precipitation peak time during their Frequent Period.  
333 The diurnal variations and the responses of precipitation peak time to aerosol are similar to that of the  
334 precipitation start time. By comparing the diurnal variations of precipitation peak time under polluted  
335 and clean conditions, we find that although the aerosols can advance or delay the precipitation time, the  
336 diurnal variation pattern has not been changed. Based on the almost fixed patterns, we can quantify the  
337 impacts of aerosol on the precipitation start and peak time. As shown earlier, we can investigate the  
338 crest of the precipitation start and peak time to quantify the influence of aerosol on the precipitation,  
339 but this method is not always suitable. As shown in Figure 6d, the crests of the peak time are at 15:00  
340 and 18:00 LT under polluted and clean conditions during the Frequent Period respectively, which  
341 suggests that the aerosol has caused the precipitation peak time 3 hours advanced in NCP. However, by  
342 comparing the diurnal variations of precipitation peak time between polluted and clean conditions, we  
343 find that there are secondary crests of precipitation peak time at 17:00 and 16:00 LT under the polluted  
344 and clean conditions respectively, which suggests that the aerosol has caused the precipitation peak  
345 time 1 hour advanced. Anyway, what we can confirm from Figure 6d is that the high frequency of the



precipitation peak time is at 15:00-17:00 LT under polluted condition while at 16:00-18:00 LT under clean condition. During the Infrequent Period over NCP, there are relatively more precipitation under polluted condition than under clean condition before sunrise, while there are relatively less precipitation under polluted condition after sunrise. Also, the precipitation peak time is 1 hour delayed (advanced) over NCP under polluted condition after (before) sunrise during the Infrequent Period of precipitation.

The crests of the precipitation peak time are both at 16:00 LT under polluted and clean conditions over YRD during the Frequent Period, which suggests that the aerosols show negligible impact on the precipitation peak time. In contrast, it shows that the precipitation peak time is 1 hour advanced under polluted condition during the Infrequent Period over YRD. The diurnal variations of the precipitation peak time are similar to that of the precipitation start time both under polluted and clean conditions over PRD. The precipitation peak time over PRD has been 2 hours delayed during the Frequent Period and 1 hour advanced during the Infrequent Period (before sunrise) by aerosols. The responses of precipitation start and peak time to aerosol are similar with each other. Consistent with the fact that the precipitation peak time appears 1-2 hours after the precipitation start time as shown in Figure 5, the crest of the precipitation peak time is also later than that of the precipitation start time as shown in Figure 6.

The findings above show that the aerosols have distinct impacts on the precipitation start time in NCP (advanced), YRD (no influence), and PRD (delayed), which may be related to their different aerosol amount and types, precipitation types, or meteorological conditions. Among the three study regions, the most polluted area is NCP and the cleanest area is PRD. Meanwhile, the proportion of the absorbing aerosol is the highest in NCP and is the lowest in PRD. Both aerosol concentration and the proportion of the absorbing aerosol in YRD are between NCP and PRD, based on which the mechanism that aerosol impacts the precipitation over YRD should include that over both NCP and PRD if the aerosols do have significant impacts on precipitation. The initial time of the Frequent Period in NCP (14:00 LT) is later than that in PRD (11:00 LT), which is most likely due to the high aerosol concentration in NCP. The high aerosol concentration reduces the solar radiation reaching the ground, making the convection suppressed in the morning in NCP. However, the high proportion of absorbing aerosol can advance the precipitation start time by strengthening the convection in the afternoon. In contrast, the scattering dominant aerosol can cool the ground surface and then low atmosphere by scattering solar radiation,



376 which weakens the convection and generally delays the precipitation start time during the Frequent  
377 Period in PRD. We also find that the aerosol makes the precipitation more frequent at night in NCP,  
378 which is most likely associated with the fact that the aerosol can heat the atmosphere and strengthen  
379 convection even after sunset due to the relatively high proportion of absorbing aerosol in NCP. In  
380 addition to aerosols, we also find that the variation of meteorology can play a role to the change of  
381 precipitation. For example, the decreasing temperature and increasing humidity are both contributable  
382 to the growth of cloud droplets and then precipitation at night. After sunrise, the precipitation seems  
383 more influenced by solar radiation and aerosols in NCP. The atmosphere is heated more quickly under  
384 clean condition than under polluted condition in the morning in NCP, making the probability of  
385 precipitation higher under clean condition in the morning.

386 The precipitation is also affected by solar radiation and aerosols after sunrise in YRD, but the aerosols  
387 show no significant influence on the precipitation start time likely due to weak radiative effect by the  
388 relatively low aerosol amount over this study region. Even with weak radiative effect due to relatively  
389 low aerosol amount, the aerosol still makes the precipitation more frequent in the afternoon and more  
390 infrequent in the morning and at night over YRD, which likely suggests the significant aerosol  
391 microphysical effect on the precipitation. Aerosols, by serving as cloud condensation nuclei, increase  
392 the cloud droplet number concentration and decrease cloud droplet sizes, decreasing the stratiform  
393 precipitation that occurs more in the morning and invigorating the convective precipitation that occurs  
394 more in the afternoon.

395 To further understand whether the different precipitation types cause distinct responses of precipitation  
396 to aerosols, we next investigate the impacts of aerosol on convective and stratiform precipitation using  
397 the same method. Note that we ignore some hours in a day, at which the sample size is too small (less  
398 than 10) to be analyzed reliably and we only investigate the impacts of aerosol on convective and  
399 stratiform precipitation during the continuous period of precipitation.

400 Figure 7 shows the PDFs of convective (stratiform) precipitation start time under polluted (red line)  
401 and clean (blue line) conditions. Figs. 7a-c show that the convective precipitation occurs frequently at  
402 time around 8:00, 12:00-14:00, and around 18:00-20:00 LT, and infrequent at 15:00-16:00 LT and at  
403 night in NCP. The aerosols advance convective precipitation start time 1-2 hours during 10:00-15:00 LT,  
404 while show no obvious influence during the periods 0:00-9:00 LT and 16:00-20:00 LT in NCP.  
405 Consistent with the results presented above, aerosol makes the precipitation more accumulated in the



afternoon, particularly at days when the aerosol radiative effect works strongly. The convective precipitations are found frequently at 9:00-15:00 LT in YRD. The crest of convective precipitation start time is both at 12:00 LT under polluted and clean conditions during the period 8:00-16:00 LT in YRD, while it is delayed by 1 hour by aerosols during the period 13:00-16:00 LT. The continuous period with enough precipitation samples is 7:00-22:00 LT in PRD. The convective precipitation start time over PRD shows negligible response to aerosols during the period 7:00-11:00 LT, while is 1 hour delayed during the period 12:00-22:00 LT. As shown in Figure 7c, the crest and secondary crest of the convective precipitation start time are at 12:00 and 17:00 LT under clean condition and at 14:00 and 18:00 LT under polluted condition, which implies that the delaying effect of aerosols on convective precipitation start time becomes weaker with the decreasing solar radiation or convective strength. Figs. 7d-f show the stratiform precipitation occurs frequently at night and around sunrise with a peak occurrence frequency at about 7:00 LT in NCP. The aerosol shows no significant influence on the start time of the stratiform precipitation in NCP. In YRD, the diurnal variations of the stratiform precipitation start time are similar under polluted and clean conditions, while the occurrence frequencies at a given hour are slightly different, which indicates that the aerosol can only weakly affect the stratiform precipitation start time. In PRD, more stratiform precipitation occurs in the afternoon under polluted condition. Moreover, the crests of the stratiform precipitation start time are at 19:00 and 17:00 LT under clean and polluted conditions in the afternoon, respectively, which suggests that the aerosol could advance the stratiform precipitation start time by 2 hours in PRD. Figure 8 shows the PDFs of the convective and stratiform precipitation peak time under polluted and clean conditions. Note that only the continuous periods with >10 precipitation events at each given hour are investigated. The continuous periods with convective precipitation are 0:00-15:00 LT and 17:00-22:00 LT in NCP. As shown in Figure 8a, the crests of the convective precipitation peak time are at 13:00 LT (polluted condition) and 15:00 LT (clean condition) in NCP, which suggests that the aerosol could advance the convective precipitation peak time by 2 hours during the period 0:00-15:00 LT. However, it is challenging to identify whether the convective precipitation peak time has been changed by aerosols during the period 17:00-22:00 LT because of the discontinuous distribution of convective precipitation in NCP. The convective precipitations are frequent during the period 10:00-17:00 LT and aerosols show no significant influence on the convective precipitation peak time in YRD. For example, the crests of convective precipitation peak time are both at 14:00 LT under clean and polluted



conditions during the period 10:00-17:00 LT, one of the continuous periods with sufficient samples of convective precipitation events in YRD. Figure 8c shows that there is a continuous period of convective precipitation at 0:00-17:00 LT in PRD, during which the aerosol enhances the convective precipitation gradually. The radiative effect of aerosol generally works significantly during the period 11:00-15:00 LT, which helps advance the convective precipitation peak time by 1 hour in PRD. The frequency of the stratiform precipitation of the day fluctuates greatly in NCP, and shows larger values in the early morning and early afternoon over YRD. The stratiform precipitations are not affected by aerosols clearly over both NCP and YRD. Over PRD, the stratiform precipitation is also strengthened gradually by aerosol, while the stratiform precipitation peak time is likely 1 hour delayed by aerosols during the period 13:00-21:00 LT. It is clear that the aerosol affects the convective precipitation much more strongly than the stratiform precipitation over NCP and YRD, while the aerosol shows different impacts on convective and stratiform precipitation over PRD. Due to the high proportion of the stratiform precipitation over PRD, the start and peak time of total precipitation events are delayed, as shown in Figure 6.

The above findings have suggested that the aerosol can affect convection, and we next try to confirm this hypothesis. If the aerosol could affect precipitation and convection, the temperature and vertical velocity would show strong responses to the changes of aerosol over the plain regions. We here investigate how the temperature and vertical velocity change with aerosol concentration and type at different pressure levels. The differences of temperature between polluted and clean conditions are shown in Figure 9a-c. As shown, the aerosol causes significant changes of atmospheric temperature by radiative effect at low troposphere (1000-900 hPa). As the altitude increases, the aerosol radiative effect decreases gradually which results in smaller temperature differences. The strongest influence of aerosol on temperature is shown in NCP and the weakest is in PRD, which is likely related to their difference in aerosol amount. It is also clear that the aerosol heats the atmosphere all day in NCP.

As shown in Figure 9a, the radiative effect of aerosol is strengthened gradually after the sunrise with the largest impact on atmospheric temperature at 19:00-22:00 LT and gets weakened from midnight to before sunrise the next day in NCP, which implies that the precipitations are also affected by the aerosol radiative effect at night. The atmosphere is heated by aerosols over YRD for almost all time except the period 3:00-6:00 LT. The radiative effect of aerosol increases after sunrise and decreases after sunset with the largest impact on atmospheric temperature at 15:00-18:00 LT in YRD. The





obvious cooling effect of aerosol is shown in PRD for almost all time except for a weak heating effect in the morning. After sunrise, the cooling effect increases gradually in PRD. The above phenomena could help explain why the aerosol shows different influence on the precipitation start and peak time over the three study regions. Over the NCP, the impacts of aerosol radiative effect on atmospheric temperature at 1000-950 hPa is weaker than that at 925-875 hPa, implying that the potential convective energy need time to accumulate. Correspondingly, the convection is strengthened weakly in the morning even though the aerosol can heat the atmosphere due to the high aerosol concentration. Accompanied by the accumulation of aerosol heating effect with time, the aerosols favor the convection strongly and then advance the precipitation start time over the NCP. Differently, the aerosols paly a cooling effect over the PRD, and accompanied by the accumulated aerosol cooling effect with time, the precipitation start time is delayed.

Figure 9d-f show the differences in vertical velocity between polluted and clean conditions, which further confirms the above results. The positive vertical velocity (downward movement) suppresses the convection and the negative (upward movement) strengthens the convection. In general, when the aerosol heats (cools) the atmosphere, the airflow is updraft (downdraft). However, we should note when the radiative effect of aerosol is weak (at night and in the early morning), the increasing temperature does not mean that the airflow must be updraft.

### 3.3 Sensitivities of aerosol impacts on precipitation to meteorological factors

In addition to aerosols, meteorological variables can also affect the precipitation. We here investigate the potential impacts from the meteorological variables, and further investigate the aerosol impacts on precipitation by limiting the influence from those meteorological variables. This study selects three crucial factors for the precipitation formation and development, including moisture, wind shear and low troposphere stability (Fan et al., 2009; Guo et al., 2016; Klein, 1997; Slingo, 1987; Zhou et al., 2020). Figures S1-S3 show the influence of moisture, WS and LTS on precipitation. Sufficient moisture is beneficial to precipitation generation and advances precipitation. The differences in precipitation frequency between crest and valley under high humidity condition are less than that under low humidity condition, which means that high moisture increases the precipitation frequency for all corresponding time instead of making precipitation gathered at a particular time range. As a result, the high humidity weakens the diurnal variations of precipitation frequency. The LTS changes the diurnal



characteristics of the precipitation start time. The precipitation is more frequent in the daytime with peak occurrence frequency in the afternoon under low LTS condition, while the precipitation is more frequent at the nighttime with valley occurrence frequency in the afternoon under high LTS condition. The high WS delays the precipitation start time by 3 hours in NCP, delays the precipitation start time by 1 hour in YRD, and advances the precipitation start time by 2 hours in PRD, which is opposite to the influence of aerosol on precipitation start time. Therefore, the high WS inhibits the aerosol effects on precipitation, which is in good agreement with the findings by Fan et al. (2009) that increasing aerosol concentrations can enhance convection under weak wind shear condition.

Using the similar method to classify meteorological conditions as aerosols, this study next investigates the differences of crest or valley of precipitation frequency between polluted and clean conditions to verify the aerosol effects by limiting the meteorological conditions. Under high humidity condition, the diurnal variations of precipitation frequency are more complicated under polluted condition over the NCP and YRD, making it challenging to judge the corresponding crest and valley time. Moreover, the aerosol radiative effect is weak under high humidity condition, which could also make the impacts of aerosols on precipitation hard to identify. Under low humidity condition, the aerosols advance the precipitation start time by 3 hours in NCP and by 1 hour in YRD. The aerosols delay the precipitation start time by 2 hours both under low and high humidity conditions in PRD. However, the differences of PDFs between polluted and clean conditions under low humidity condition are more distinct than that under high humidity condition over the PRD, which indicates that the aerosol effects on precipitation are more significant under low humidity condition. All above results suggest that the humidity can affect the strength of aerosol impacts on precipitation. The aerosol impacts on precipitation are more obvious under low humidity condition and are somehow weakened under high humidity condition. The response of aerosol impacts on precipitation peak time to humidity is basically consistent with that of the aerosol impacts on precipitation start time, but shows weakened aerosol impacts under high humidity condition more clearly, especially in PRD. Under low humidity condition, the crest of precipitation peak time is at 14:00 LT under clean condition and at 16:00 LT under polluted condition, suggesting that the precipitation peak time is 2 hours delayed by aerosols in PRD. Differently, under high humidity condition, the crests of precipitation peak time are both at 15:00 LT under both polluted and clean conditions, which suggests that the aerosols have no obvious influence on precipitation peak time under high humidity condition in PRD.



Figure 11 shows that the aerosol effects on precipitation are distinct under low LTS condition but are almost negligible under high LTS condition. The aerosols make the precipitation start time in NCP and YRD 1 hour advanced under low LTS condition. During the Frequent Period of precipitation, the frequency of precipitation under polluted condition is higher than that under clean condition, which means that the aerosol microphysical effect is prominent in addition to the aerosol radiative effect. The precipitation start time is 2 hours delayed (polluted: 16:00 LT, clean: 14:00 LT) by aerosol in PRD. The response of precipitation peak time to the aerosols are generally consistent with that of precipitation start time under different LTS conditions. The aerosol impacts on precipitation are distinct under high and low WS conditions while they are more obvious under low WS condition. In the NCP, the aerosols advance the precipitation start time under both low and high WS conditions, which suggests that the aerosol radiative effect plays significant role. However, under low WS condition, the crest frequency of precipitation under polluted condition is higher than that under clean condition in NCP, while contrary phenomenon is found under high WS condition, which suggests that the high WS suppresses the aerosol microphysical effects. The aerosols make the precipitation start time 1 hour earlier under low WS condition in YRD while the aerosol effects on precipitation start time are not obvious under high WS condition. The aerosols delay the precipitation start time under both low and high WS conditions in PRD. The responses of precipitation peak time to aerosols are also found generally consistent with that of precipitation start time under different WS conditions.

## 4. Summary and discussion

### 4.1 Summary

This study investigates the influence of aerosol on the precipitation start and peak time over three different megacity regions using the high-resolution precipitation, aerosol, and meteorological datum in summer (June-August) during the period from 2015 to 2020. We first examine the changes of precipitation start and peak time with aerosols over the North China Plain (NCP), the Yangtze River Delta (YRD), and Pearl River Delta (PRD) regions. Then we classify the precipitation into convective and stratiform precipitation types, and examine their different responses in start and peak time to aerosols. Finally, considering that meteorological variables, particularly three key meteorological variables of humidity, low tropospheric stability, and wind shear, also play important roles to



precipitation development, we further classify the meteorological conditions using the same method as aerosols and examine the aerosol impacts on precipitation start and peak time under different meteorological conditions. New findings have been provided with the following several key points.

1) The Frequent Period of precipitation start time is delayed and prolonged by high aerosol concentrations and relatively high proportion of absorbing aerosol in NCP, so the initial time of the Frequent Period in NCP (14:00 LT) is later than that in YRD (11:00 LT) and PRD (11:00 LT) while the durations of Frequent Periods are similar among the three study regions. The different aerosol concentrations and aerosol types (absorbing versus scattering) contribute to the different aerosol impacts on the precipitation start (peak) time over the NCP, YRD and PRD. The precipitation start time is 3 hours advanced in NCP but 2 hours delayed in PRD by aerosols during the Frequent Period and the precipitation start time in YRD shows negligible response to aerosol. The most likely reason is that the aerosol heats the atmosphere strongly in NCP, associated with the high aerosol concentration and the relatively larger proportion of absorbing aerosol over the NCP. The aerosol concentration and aerosol type in PRD is opposite to that in NCP. The aerosol concentration and aerosol type in YRD both are between that in NCP and PRD, and the aerosol impacts on the precipitation start (peak) time in YRD are also between that in NCP and PRD, which is relatively weakly affected by aerosol. The influences of aerosol radiative effect on precipitation start (peak) time are also found different during the different periods of the day.

2) The frequency of stratiform precipitation is higher than that of convective precipitation, but the convective precipitation is more sensitive to aerosol than stratiform precipitation. The responses of the convective precipitation start and peak time to aerosol are similar to each other with the results as shown above in point 1), except that the start time is 1 hour delayed in YRD, but the peak time is 1 hour advanced in PRD.

3) Humidity is beneficial to precipitation which can advance the precipitation start (peak) time, but the influence of aerosol on precipitation is weakened when the humidity is high. The low tropospheric stability (LTS) can modify the diurnal variation characteristics of precipitation start (peak) time. The influences of aerosol on precipitation start time are more significant under low LTS. Vertical wind shear (WS) inhibits the aerosol effects on precipitation, since the influences of WS on the precipitation start (peak) time are opposite to that of aerosols. WS delays the precipitation start (peak) time by 3 hours in NCP and by 1 hour in YRD, while advances the precipitation start (peak) time by 2 hours in



583 PRD.

## 584 4.2 Discussion

585 The aerosol-precipitation interaction is a hot topic in atmospheric science and has many challenges due  
586 to its complexity. Previous studies have focused on the influence of aerosols on the precipitation  
587 intensity at inter-decadal or daily time scales, but few studies have examined the impacts of aerosols on  
588 the precipitation time for a large amount of precipitation events. This study investigates the impacts of  
589 aerosols on the precipitation start and peak time for both stratiform and convective precipitations by  
590 limiting the impacts of meteorological variables, which are essential for improve our understanding of  
591 aerosol-precipitation interaction. However, there are still some problems in current study, with at least  
592 the following several points.

593 First, the temporal resolution of observations is still too coarse for current study. For example, the  
594 temporal resolution of precipitation product is 1 hour in this study, which makes it difficult for us to  
595 more accurately quantify the impact of aerosols on precipitation time: precipitation time changes with  
596 values less than 1 hour are not able to be identified. Second, the complicated mechanisms and  
597 processes of aerosol effect on precipitation could introduce extra uncertainties to our findings.  
598 Currently, we only examine the sensitives of aerosol effects on precipitation under different humidity,  
599 LTS and WS conditions, which might be not sufficient. Also, this study focuses on summer  
600 precipitation, but the influence of summer monsoon has not been considered and definitely need be  
601 investigated further in future. Finally, we would like to mention that we focus on the aerosol radiative  
602 effects on precipitation time while the aerosol microphysical effect is less discussed. It is hard to  
603 distinguish radiative effect and microphysical effect using observation study alone, so the numerical  
604 model simulations should be applied further in future. Moreover, the influence of aerosol on  
605 precipitation intensity and duration also need to be investigated deeply further over different regions.

606 **Data availability.** Surface elevation data from the Shuttle Radar Topography Mission (SRTM) were  
607 downloaded from <http://srtm.csi.cgiar.org/> (Yang et al., 2021). ERA-5 Reanalysis data were provided  
608 by the European Centre for Medium Weather Forecasts (<https://cds.climate.copernicus.eu/>, Fan et al.,  
609 2020). The hourly precipitation data from China Merged Precipitation Analysis Version 1.0 product can  
610 be downloaded in real time from the <http://cdc.cma.gov.cn/sksj.do?method=ssrjscprh> (Shen et al.,



2014). The hourly PM<sub>2.5</sub> mass concentration provided by the China Environmental Monitoring Station of the national air quality real time release platform with data quality assurance (<http://beijingair.sinaapp.com>, Sun et al., 2019). The DPR Level-2A product from the Global Precipitation Measurement (GPM) mission can be downloaded from <https://gpm.nasa.gov/missions/GPM> (Zhang et al., 2018).

**Author contributions.** CFZ and YS developed the ideas and designed the study. YS contributed to collection and analyses of data. YS performed the analysis and prepared the manuscript. CFZ supervised and modified the manuscript. All authors made substantial contributions to this work.

**Competing interests.** The authors declare that they have no conflict of interest.

**Acknowledgements.** This work was supported by the Ministry of Science and Technology of China National Key Research and Development Program (2017YFC1501403), the National Natural Science Foundation of China (41925022, 41575143), the State Key Laboratory of Earth Surface Processes and Resources Ecology, and the Fundamental Research Funds for the Central Universities.

## Reference

- Ackerman, A. S., Toon, O. B., Stevens, D. E., Heymsfield, A. J., Ramanathan, V. and Welton, E. J.: Reduction of Tropical Cloudiness by Soot, *Science*, 288(5468), 1042, <https://doi.org/10.1126/science.288.5468.1042>, 2000.
- Albrecht, B. A.: Aerosols, cloud microphysics, and fractional cloudiness, *Science*, 245(4923), 1227-1230, <https://doi.org/10.1126/science.245.4923.1227>, 1989.
- An, Z., Huang, R. J., Zhang, R., Tie, X., Li, G., Cao, J., Zhou, W., Shi, Z., Han, Y., and Gu, Z.: Severe haze in northern China: A synergy of anthropogenic emissions and atmospheric processes, *Proc. Natl. Acad. Sci. U.S.A.*, 116(18), 8657–8666. <https://doi.org/10.1073/pnas.1900125116>, 2019.
- Andreae, M. O., Rosenfeld, D., Artaxo, P., Costa, A. A., Frank, G. P., Longo, K. M. and Silva-Dias, M. A. F.: Smoking Rain Clouds over the Amazon, *Science*, 303(5662), 1337-1342, <https://doi.org/10.1126/science.1092779>, 2004.



- 636 Boucher, O. and Quaas, J.: Water vapour affects both rain and aerosol optical depth, *Nat. Geosci.*, 6,  
 637 4–5, <https://doi.org/10.1038/ngeo1692>, 2012.
- 638 Che, H., Qi, B., Zhao, H., Xia, X., Eck, T. F., Goloub, P., Dubovik, O., Estelles, V., Cuevas-Agulló, E.,  
 639 Blarel, L., Wu, Y., Zhu, J., Du, R., Wang, Y., Wang, H., Gui, K., Yu, J., Zheng, Y., Sun, T., Chen,  
 640 Q., Shi, G., and Zhang, X.: Aerosol optical properties and direct radiative forcing based on  
 641 measurements from the China Aerosol Remote Sensing Network (CARSNET) in eastern China,  
 642 *Atmos. Chem. Phys.*, 18, 405–425, <https://doi.org/10.5194/acp-18-405-2018>, 2018.
- 643 Chen, H., Gu, X. F., Cheng, T. H., Yu, T. and Li, Z. Q.: Characteristics of aerosol types over China, *J.*  
 644 *Remote Sens.*, 17(6):1559–1571, <https://doi.org/10.11834/jrs.20133028>, 2013.
- 645 Chen, H. Q., Lu, D. K., Zhou, Z. H., Zhu, Z. W., Ren, Y. J., Yong, B.: An overview of assessments on  
 646 global precipitation measurement (GPM) precipitation products, *Water Resour. Protect.*, 35(1):  
 647 27–34, <https://doi.org/10.3880/j.issn.1004-6933.2019.01.006>, 2019, (in Chinese).
- 648 Chen, W. D., Fu, D. H., Miao, S. G., and Zhang, Y. Z.: Impacts of aerosols from Beijing and the  
 649 surrounding areas on urban precipitation, *Chin. Sci. Bull.*, 60:2124–2135,  
 650 <https://doi.org/10.1360/N972015-00217>, 2015, (in Chinese).
- 651 Chen, Y. X.: Analysis of aerosol types and sources in the typical pollution region of China based on  
 652 MODIS product, Nanjing University of Information Science and Technology, Master thesis, 2014.
- 653 Ding, A., Huang, X., Nie, W., Chi, X., Xu, Z., Zheng, L., Xu, Z., Xie, Y., Qi, X., Shen, Y., Sun, P.,  
 654 Wang, J., Wang, L., Sun, J., Yang, X.-Q., Qin, W., Zhang, X., Cheng, W., Liu, W., Pan, L., and Fu,  
 655 C.: Significant reduction of PM<sub>2.5</sub> in eastern China due to regional-scale emission control:  
 656 evidence from SORPES in 2011–2018, *Atmos. Chem. Phys.*, 19, 11791–11801,  
 657 <https://doi.org/10.5194/acp-19-11791-2019>, 2019.
- 658 Edenhofer, O. and Seyboth, K.: Intergovernmental Panel on Climate Change (IPCC), *Encyclopedia of*  
 659 *Energy, Natural Resource, and Environ. Econ.*, 1:48–56,  
 660 <https://doi.org/10.1016/B978-0-12-375067-9.00128-5>, 2013.
- 661 Fan, H., Wang, Y., Zhao, C., Yang, Y., Yang, X., Sun, Y., and Jiang, S.: The role of primary emission  
 662 and transboundary transport in the air quality changes during and after the COVID-19 lockdown  
 663 in China, *Geophys. Res. Lett.*, 48, e2020GL091065, <https://doi.org/10.1029/2020GL091065>,  
 664 2021.
- 665 Fan, J., Leung, L. R., Rosenfeld, D., Chen, Q., Li, Z., Zhang, J. and Yan, H.: Microphysical effects



determine macrophysical response for aerosol impacts on deep convective clouds, *Proc. Natl. Acad. Sci. U.S.A.*, 110(48), E4581, <https://doi.org/10.1073/pnas.1316830110>, 2013

Fan, J., Rosenfeld, D., Ding, Y., Leung, L. R. and Li, Z.: Potential aerosol indirect effects on atmospheric circulation and radiative forcing through deep convection, *Geophys. Res. Lett.*, 39(9), L09806, <https://doi.org/10.1029/2012GL051851>, 2012.

Fan, J., Rosenfeld, D., Yang, Y., Zhao, C., Leung, L. R. and Li, Z.: Substantial contribution of anthropogenic air pollution to catastrophic floods in Southwest China, *Geophys. Res. Lett.*, 42(14), 6066-6075, <https://doi.org/10.1002/2015GL064479>, 2015.

Fan, J., Yuan, T., Comstock, J. M., Ghan, S., Khain, A., Leung, L. R., Li, Z., Martins, V. J. and Ovchinnikov, M.: Dominant role by vertical wind shear in regulating aerosol effects on deep convective clouds, *J. Geophys. Res. Atmos.*, 114(D22), <https://doi.org/10.1029/2009JD012352>, 2009.

Fan, J. W., Rosenfeld, D., Zhang, Y. W., Giangrande, S. E., Li, Z. Q., Machado, L. A. T., Martin, S. T., Yang, Y., Wang, J., Artaxo, P., Barbosa, H. M. J., Braga, R. C., Comstock, J. M., Feng, Z., Gao, W. H., Gomes, H. B., and Mei, F.: Substantial convection and precipitation enhancements by ultrafine aerosol particles, *Science*, 359, 411–418, <https://doi.org/10.1126/science.aan8461>, 2018.

Garrett, T. J. and Zhao, C.: Increased Arctic cloud longwave emissivity associated with pollution from mid-latitudes, *Nature*, 440(7085), 787-789, <https://doi.org/10.1038/nature04636>, 2006.

Guo, J., Deng, M., Lee, S. S., Wang, F., Li, Z., Zhai, P., Liu, H., Lv, W., Yao, W., and Li, X.: Delaying precipitation and lightning by air pollution over the Pearl River Delta. Part I: Observational analyses, *J. Geophys. Res. Atmos.*, 121, 6472–6488, <https://doi.org/10.1002/2015JD023257>, 2016.

He, X., Lu, C. S., and Zhu, J.: A study of the spatiotemporal variation in aerosol types and their radiation effect in China, *Acta Scientiae Circumstantiae*, <https://doi.org/10.13671/j.hjkxxb.2020.0100>, 40(11): 4070-4080, 2020, (in Chinese).

Hoffmann, L., Günther, G., Li, D., Stein, O., Wu, X., Griessbach, S., Heng, Y., Konopka, P., Müller, R., Vogel, B., and Wright J. S.: From ERA - Interim to ERA5: The considerable impact of ECMWF's next - generation reanalysis on Lagrangian transport simulations, *Atmos. Chem. Phys.*, 19(5), 3097-3124, <https://doi.org/10.5194/acp-19-3097-2019>, 2019.

Huang, J., Lin, B., Minnis, P., Wang, T., Wang, X., Hu, Y., Yi, Y. and Ayers, J. K.: Satellite-based assessment of possible dust aerosols semi-direct effect on cloud water path over East Asia,





- 696 Geophys. Res. Lett., 33(19), <https://doi.org/10.1029/2006GL026561>, 2006a.
- 697 Huang, J., Minnis, P., Lin, B., Wang, T., Yi, Y., Hu, Y., Sun-Mack, S. and Ayers, K.: Possible influences  
 698 of Asian dust aerosols on cloud properties and radiative forcing observed from MODIS and  
 699 CERES, Geophys. Res. Lett., 33(6), <https://doi.org/10.1029/2005GL024724>, 2006b.
- 700 Huang, J., Minnis, P., Yan, H., Yi, H., Chen, B., Zhang, L. and Ayers, J.: Dust aerosol effect on  
 701 semi-arid climate over Northwest China detected from A-Train satellite measurements, Atmos.  
 702 Chem. Phys., 10, <https://doi.org/10.5194/acp-10-6863-2010>, 2010.
- 703 Khain, A., Rosenfeld, D. and Pokrovsky, A.: Aerosol impact on the dynamics and microphysics of deep  
 704 convective clouds, Q. J. R. Meteorol. Soc., 131(611), 2639-2663, <https://doi.org/10.1256/qj.04.62>,  
 705 2010.
- 706 Klein, S. A.: Synoptic variability of low-cloud properties and meteorological parameters in the  
 707 subtropical trade wind boundary layer, J. Climate, 10, 2018-2039,  
 708 [https://doi.org/10.1175/1520-0442\(1997\)010<2018:svolcp>2.0.co;2](https://doi.org/10.1175/1520-0442(1997)010<2018:svolcp>2.0.co;2), 1997.
- 709 Koren, I., Kaufman, Y. J., Rosenfeld, D., Remer, L. A. and Rudich, Y.: Aerosol invigoration and  
 710 restructuring of Atlantic convective clouds, Geophys. Res. Lett., 32(14),  
 711 <https://doi.org/10.1029/2005GL023187>, 2005.
- 712 Lebo, Z. and Morrison, H.: Dynamical Effects of Aerosol Perturbations on Simulated Idealized Squall  
 713 Lines, Mon. Wea. Rev., 142 (3), 991-1009, <https://doi.org/10.1175/MWR-D-13-00156.1>, 2014.
- 714 Lee, S. S., Guo, J. and Li, Z.: Delaying precipitation by air pollution over the Pearl River Delta: 2.  
 715 Model simulations, J. Geophys. Res. Atmos., 121, 11, 739–11, 760,  
 716 <https://doi.org/10.1002/2015JD024362>, 2016.
- 717 Li, Z., Niu, F., Fan, J., Liu, Y., Rosenfeld, D. and Ding, Y.: Long-term impacts of aerosols on the  
 718 vertical development of clouds and precipitation, Nat. Geosci., 4(12), 888-894,  
 719 <https://doi.org/10.1038/ngeo1313>, 2011.
- 720 Lin, J. C., Matsui, T., Pielke Sr., R. A. and Kummerow, C.: Effects of biomass-burning-derived aerosols  
 721 on precipitation and clouds in the Amazon Basin: a satellite-based empirical study, J. Geophys.  
 722 Res. Atmos., 111(D19), <https://doi.org/10.1029/2005JD006884>, 2006.
- 723 Niu, F. and Li, Z.: Systematic variations of cloud top temperature and precipitation rate with aerosols  
 724 over the global tropics, Atmos. Chem. Phys., 12(18), 8491-8498,  
 725 <https://doi.org/10.5194/acp-12-8491-2012>, 2012.



- 2726 Pincus, R., and Baker, M. B.: Effect of precipitation on the albedo susceptibility of clouds in the marine  
 2727 boundary layer, *Nature*, 372(6503):250-252, <https://doi.org/10.1038/372250a0>, 1994.
- 2728 Qiu, Y., Zhao, C., Guo, J. and Li, J.: 8-Year ground-based observational analysis about the seasonal  
 2729 variation of the aerosol-cloud droplet effective radius relationship at SGP site, *Atmos. Environ.*,  
 2730 164, 139-146, <https://doi.org/10.1016/j.atmosenv.2017.06.002>, 2017.
- 2731 Rosenfeld, D.: Suppression of Rain and Snow by Urban and Industrial Air Pollution, *Science*,  
 2732 287(5459), 1793, <https://doi.org/10.1126/science.287.5459.1793>, 2000.
- 2733 Rosenfeld, D., Lohmann, U., Raga, G. B., Dowd, C. D., Kulmala, M., Fuzzi, S., Reissell, A. and  
 2734 Andreae, M. O.: Flood or Drought: How Do Aerosols Affect Precipitation? *Science*, 321(5894),  
 2735 1309, <https://doi.org/10.1126/science.1160606>, 2008.
- 2736 Shen, Y., Zhao, P., Pan, Y. and Yu, J.: A high spatiotemporal gauge-satellite merged precipitation  
 2737 analysis over China, *J. Geophys. Res. Atmos.*, 119, 3063-3075,  
 2738 <https://doi.org/10.1002/2013JD020686>, 2014.
- 2739 Shi, R., Wang, T. J., Li, S., Zhuang, B. L., Jiang, Z. Q., Liao, J. B., Yin, C. Q.: The Spatial and  
 2740 Temporal Characteristics of Aerosol-Cloud-Precipitation Interactions during Summer in East Asia,  
 2741 *Chinese J. Atmospheric Sci.*, 2015, 39(1): 12-22,  
 2742 <https://doi.org/10.3878/j.issn.1006-9895.1404.13276>, 2015, (in Chinese).
- 2743 Shi, X., Zhao, C., Jiang, J. H., Wang, C., Yang, X., and Yung, Y. L.: Spatial Representativeness of PM<sub>2.5</sub>  
 2744 Concentrations Obtained Using Reduced Number of Network Stations, *J. Geophys. Res. Atmos.*,  
 2745 123(6), 3145-3158, <https://doi.org/10.1002/2017JD027913>, 2018.
- 2746 Slingo, J. M.: A cloud parametrization scheme derived from gate data for use with a numerical model.  
 2747 *Q. J. R. Meteorol. Soc.*, 106(450), <https://doi.org/10.1002/qj.49710645008>, 1980.
- 2748 Slingo, J. M.: The Development and Verification of A Cloud Prediction Scheme For the Ecmwf Model,  
 2749 *Q. J. R. Meteorol. Soc.*, 113: 899-927, <https://doi.org/10.1002/qj.49711347710>, 1987.
- 2750 Song, C., He, J., Wu, L., Jin, T., Chen, X., Li, R., Ren, P., Zhang, L. and Mao, H.: Health burden  
 2751 attributable to ambient PM<sub>2.5</sub> in China, *Environ. Pollut.*, 223, 575-586,  
 2752 <https://doi.org/10.1016/j.envpol.2017.01.060>, 2017.
- 2753 Speirs, P., Gabella, M., and Berne, A.: A comparison between the GPM dual-frequency precipitation  
 2754 radar and ground-based radar precipitation rate estimates in the Swiss Alps and Plateau, *J. Hydrol.*,  
 2755 18(5): 1247-1269, <https://doi.org/10.1175/JHM-D-16-0085.1>, 2017.



- 756 Sun, Y., Zhao, C., Su, Y., Ma, Z. S., Li, J. M., Letu, H., Yang, Y. K., and Fan, H.: Distinct impacts of  
 757 light and heavy precipitation on PM<sub>2.5</sub> mass concentration in Beijing, *Earth and Space Science*, 6,  
 758 <https://doi.org/10.1029/2019EA000717>, 2019.
- 759 Tao, W.-K., Li, X., Khain, A., Matsui, T., Lang, S., and Simpson, J.: Role of atmospheric aerosol  
 760 concentration on deep convective precipitation: Cloud-resolving model simulations, *J. Geophys.*  
 761 *Res.*, 112, D24S18, <https://doi.org/10.1029/2007JD008728>, 2007.
- 762 Tao, W. K., Chen, J. P., Li, Z., Wang, C. E. and Zhang, C. D.: Impact of aerosols on convective clouds  
 763 and precipitation, *Rev. Geophys.*, 50(2), RG2001, <https://doi.org/10.1029/2011RG000369>, 2012.
- 764 Teller, A. and Levin, Z.: The effects of aerosols on precipitation and dimensions of subtropical clouds:  
 765 A sensitivity study using a numerical cloud model, *Atmos. Chem. Phys.*, 5(4):7211-7245,  
 766 <https://doi.org/10.5194/acp-6-67-2006>, 2006.
- 767 Twomey, S.: The Influence of Pollution on the Shortwave Albedo of Clouds, *J. Atmos. Sci.*, 34(7),  
 768 1149-1152, [https://doi.org/10.1175/1520-0469\(1977\)0342.0.CO;2](https://doi.org/10.1175/1520-0469(1977)0342.0.CO;2), 1977.
- 769 Urraca, R., Huld, T., Gracia - Amillo, A., Martinez - de - Pison, F. J., Kaspar, F., and Sanz - Garcia, A.:  
 770 Evaluation of global horizontal irradiance estimates from ERA5 and COSMO - REA6 reanalyses  
 771 using ground and satellite - based data. *Sol. Energy*, 164, 339–354,  
 772 <https://doi.org/10.1016/j.solener.2018.02.059>, 2018.
- 773 Wang, C.: A modeling study of the response of tropical deep convection to the increase of cloud  
 774 condensation nuclei concentration: 1. Dynamics and microphysics, *J. Geophys. Res. Atmos.*,  
 775 110(D21), <https://doi.org/10.1029/2004JD005720>, 2005.
- 776 Wang, J., Xing, J., Mathur, R., Pleim, J. E., Wang, S., Hogrefe, C., Gan, C. M., Wong, D. C. and Hao, J.  
 777 M.: Historical Trends in PM<sub>2.5</sub>-Related Premature Mortality during 1990-2010 across the Northern  
 778 Hemisphere, *Environ. Health Perspect.*, 125(3), 400-408, <https://doi.org/10.1289/EHP298>, 2017.
- 779 Wang, Y. H., Gao, W. K., Wang, S. A., Song, T., Gong, Z. Y., Ji, D. S., Wang, L. L., Liu, Z. R., Tang, G.  
 780 Q., Huo, Y. F., Tian, S. L., Li, J. Y., Li, M. G., Yang, Y., Chu, B. W., Petäjä, T., Kerminen, V.-M.,  
 781 He, H., Hao, J. M., Kulmala, M., Wang, Y. S., and Zhang, Y. H.: Contrasting trends of PM<sub>2.5</sub> and  
 782 surface-ozone concentrations in China from 2013 to 2017, *Natl. Sci. Rev.*, 7(8), 1331-1339,  
 783 <https://doi.org/10.1093/nsr/nwaa032>, 2020.
- 784 Wood, R. and Bretherton C. S.: On the relationship between stratiform low cloud cover and  
 785 lower-tropospheric stability, *J. Clim.*, 19(24), 6425-6432, <https://doi.org/10.1175/jcli3988.1>,



- 2006.
- Wu, G. X., Li, Z. Q., Fu, C. B., Zhang, X. Y., Zhang, R. Y., Zhang, R. H., Zhou, T. J., Li, J. P., Li, J. D., Zhou, D. G., Wu, L., Zhou, L. T., He, B., and Huang, R. H.: Advances in studying interactions between aerosols and monsoon in China, Science China: Earth Sciences, <https://doi.org/10.1007/s11430-015-5198-z>, 2015.
- Yang, T. J., Liu, Y. D., and Sui, M.: Impacts of different concentrations of anthropogenic pollutants on a rainstorm, Chinese J. Atmospheric Sci., 41(4): 882-896, <https://doi.org/10.3878/j.issn.1006-9895.1702.16235>, 2017, (in Chinese).
- Yang, X., Zhao, C., Zhou, L., Wang, Y. and Liu, X.: Distinct impact of different types of aerosols on surface solar radiation in China, J. Geophys. Res. Atmos., 121, 6459-6471, <https://doi.org/10.1002/2016JD024938>, 2016.
- Yang, X., Zhou, L., Zhao, C. and Yang, J.: Impact of aerosols on tropical cyclone induced precipitation over the mainland of China, Clim. Change, 148, 173-185, <https://doi.org/10.1007/s10584-018-2175-5>, 2018.
- Yang, X., Zhao, C., Yang, Y., and Fan, H.: Long-term multi-source data analysis about the characteristics of aerosol optical properties and types over Australia, Atmos. Chem. Phys., 21, 3803-3825, <https://doi.org/10.5194/acp-21-3803-2021>, 2021.
- Yang, Y., Zhao, C., Wang, Q., Cong, Z., Yang, X., and Fan, H.: Aerosol characteristics at the three poles of the Earth as characterized by Cloud-Aerosol Lidar and Infrared Pathfinder Satellite Observations, Atmos. Chem. Phys., 21, 4849-4868, <https://doi.org/10.5194/acp-21-4849-2021>, 2021.
- Zhang, A. Q. and Fu, Y. F.: The structural characteristics of precipitation cases detected by dual-frequency radar of GPM satellite, Chinese J. Atmospheric Sci., 42(1):33-51, <https://doi.org/10.3878/j.issn.1006-9895.1705.16220>, 2018, (in Chinese).
- Zhao, C. and Garrett, T.: Effects of Arctic haze on surface cloud radiative forcing, Geophys. Res. Lett., 42, 557-564, <https://doi.org/10.1002/2014GL062015>, 2015.
- Zhao, C., Lin, L., Wu, F., Wang, Y., Li, Z., Rosenfeld, D., and Wang, Y.: Enlarging Rainfall Area of Tropical Cyclones by Atmospheric Aerosols, Geophysical Research Letters, 45(16), 8604-8611, <https://doi.org/10.1029/2018GL079427>, 2018.
- Zheng, B., Tong, D., Li, M., Liu, F., Hong, C. P., Geng, G. N., Li, H. Y., Li, X., Peng, L. Q., Qi, J., Yan,



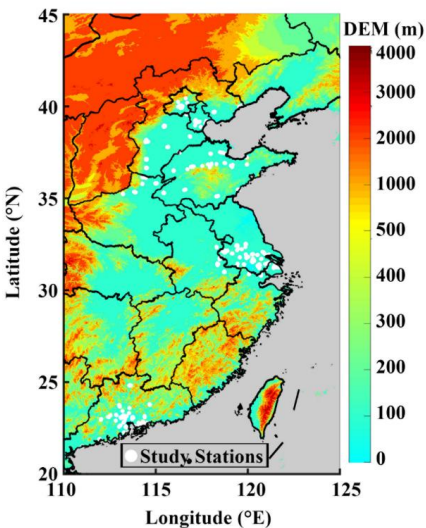
816 L., Zhang, Y. X., Zhao, H. Y., Zheng, Y. X., He, K. B., and Zhang, Q.: Trends in China's  
817 anthropogenic emissions since 2010 as the consequence of clean air actions, Atmos. Chem. Phys.,  
818 18, 14095–14111, <https://doi.org/10.5194/acp-18-14095-2018>, 2018.

819 Zhou, S. Y., Yang, J., Wang, W. C., Zhao, C. F., Gong, D. Y., and Shi, P. J.: An observational study of  
820 the effects of aerosols on diurnal variation of heavy rainfall and associated clouds over  
821 Beijing-Tianjin-Hebei, Atmos. Chem. Phys., 20, 5211–5229, 2020,  
822 <https://doi.org/10.5194/acp-20-5211-2020>, 2020.

823 **Figures and tables**

824 Table 1: The number and proportion of different types of precipitation in the three study regions of  
825 North China Plain (NCP), Yangtze River Delta (YRD), and Pearl River Delta (PRD).

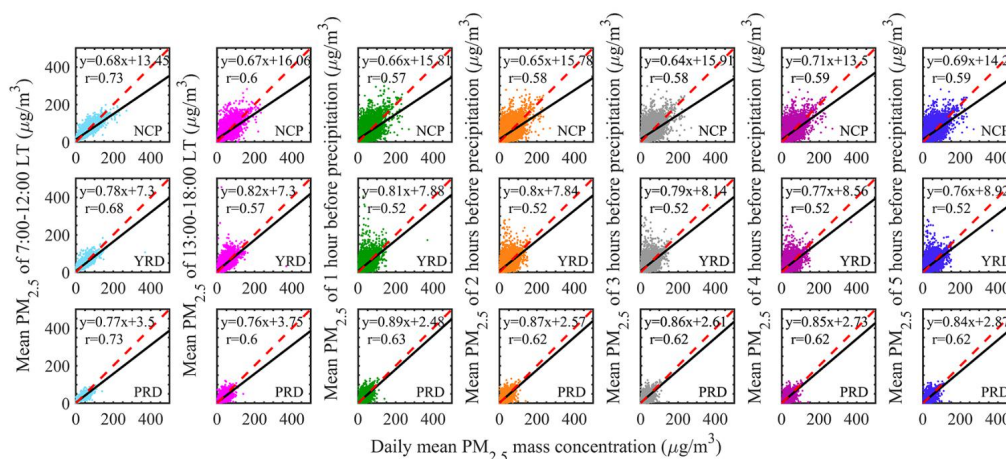
Study area	NCP	YRD	PRD
Total case numbers	21567	30659	26861
Convective case numbers (proportion %)	3362 (15.59)	6683 (21.8)	9464 (35.23)
Stratiform case numbers (proportion %)	16951 (78.6)	21104 (68.83)	15309 (56.99)
Other case numbers (proportion %)	1254 (5.81)	2872 (9.37)	2088 (7.77)



826  
827 Figure 1: The study region with surface altitude (m) information from Digital Elevation Model (DEM).  
828 The white dots are the PM<sub>2.5</sub> site stations used in this study, and the color map represents the DEM

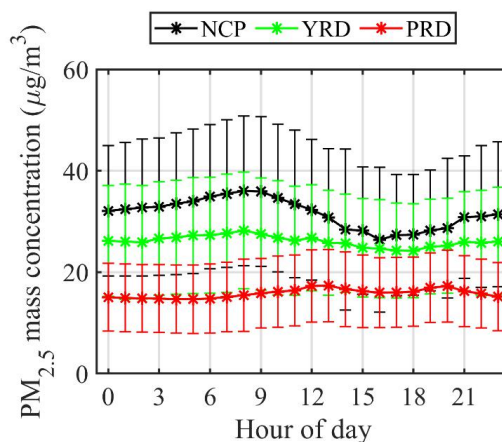


829 information.



830

831 Figure 2: The relationships between the daily mean  $\text{PM}_{2.5}$  mass concentration ( $\mu\text{g}/\text{m}^3$ ) and the mean  
 832  $\text{PM}_{2.5}$  mass concentration of 7:00-12:00 LT (azure, the first column), 13:00-18:00 LT (roseo, the second  
 833 column), 1 hour before precipitation (green, the third column), 2 hours before precipitation (orange, the  
 834 fourth column), 3 hours before precipitation (grey, the fifth column), 4 hours before precipitation  
 835 (purple, the sixth column), and 5 hours before precipitation (blue, the seventh column) in June-August  
 836 from 2015 to 2020 over North China Plain (NCP, the first row), Yangtze River Delta (YRD, the second  
 837 row), and Pearl River Delta (PRD, the third row), respectively.

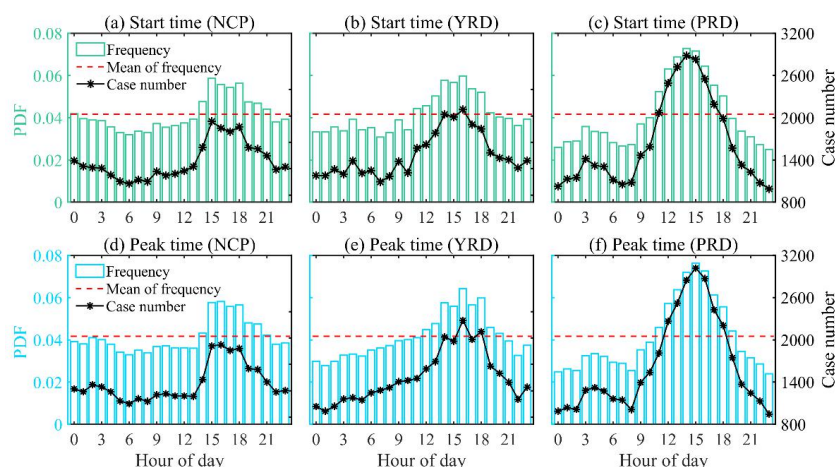


838

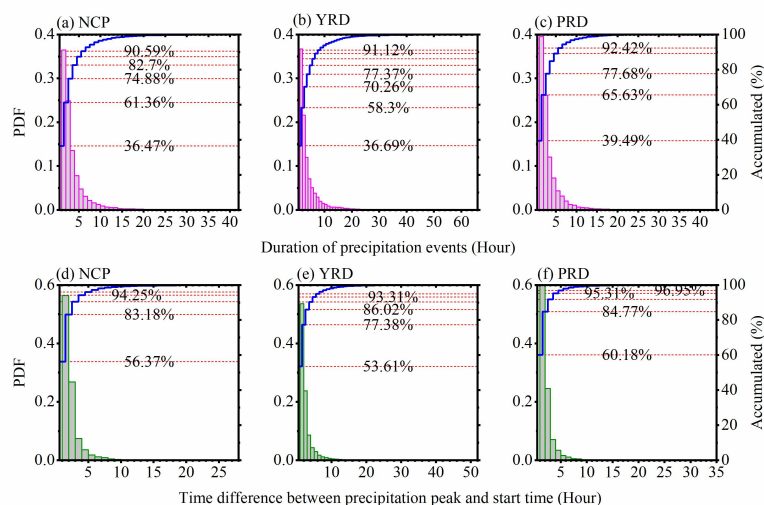
839 Figure 3: The diurnal variation of  $\text{PM}_{2.5}$  mass concentration ( $\mu\text{g}/\text{m}^3$ ) during the period of June-August  
 840 from 2015 to 2020 in North China Plain (NCP; black), Yangtze River Delta (YRD; green) and Pearl



841 River Delta (PRD, red). The dotted lines are for average values, and the vertical bars are for standard  
 842 deviations of  $PM_{2.5}$  mass concentration at each hour.  
 843



844  
 845 Figure 4: The probability density functions (PDFs) of the start time (a-c, green) of precipitation and the  
 846 peak time (d-f, blue) of precipitation in June-August from 2015 to 2020 over three study regions. The  
 847 NCP, YRD, and PRD represent North China Plain, Yangtze River Delta, and Pearl River Delta,  
 848 respectively. The black line represents the sample amount of precipitation events at the corresponding  
 849 time, and the red dotted line is the average daily precipitation frequency.

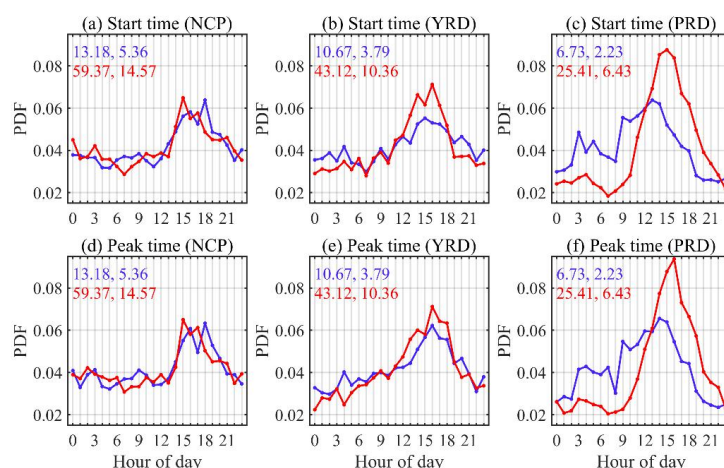


850





851 Figure 5: The PDFs of duration of precipitation events (a-c) and PDFs of time difference (in hours)  
 852 between precipitation peak and start time for all precipitation events (d-e) during the study period of  
 853 June-August from 2015 to 2020 over three study regions. The NCP, YRD, and PRD represent North  
 854 China Plain, Yangtze River Delta, and Pearl River Delta, respectively. Blue solid lines denote  
 855 accumulated occurrence frequencies of precipitation (ordinate on the right-hand side of each panel).  
 856 Red dotted lines and numbers show the accumulated occurrence frequencies of precipitation.



857  
 858 Figure 6: Normalized PDFs of precipitation (a-c) start time and (d-e) peak time (units: LT), represented  
 859 as ratios of their corresponding precipitation frequency at a given hour to those accumulated over 24 h  
 860 under clean (blue lines) and polluted (red lines) conditions in June-August from 2015 to 2020 over  
 861 NCP, YRD and PRD, respectively. The blue (red) numbers are the average (the first column) and  
 862 standard deviation (the second column) of the PM<sub>2.5</sub> mass concentration (μg/m<sup>3</sup>) under clean (polluted)  
 863 condition.



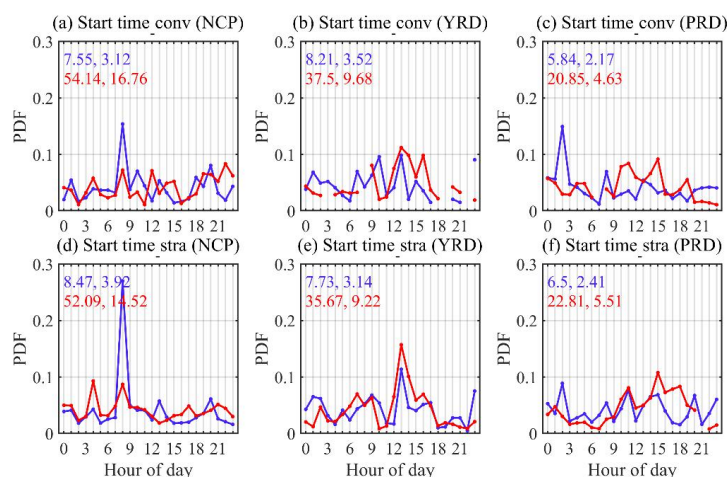


Figure 7: Normalized PDFs of (a-c) convective precipitation start time and (d-e) stratiform precipitation start time (units: LT), represented as ratios of their corresponding precipitation frequency at a given hour to those accumulated over 24 h under clean (blue lines) and polluted (red lines) conditions in June-August from 2015 to 2020 over NCP, YRD and PRD, respectively. The blue (red) numbers are the average (the first column) and standard deviation (the second column) of the PM<sub>2.5</sub> mass concentration (μg/m<sup>3</sup>) under clean (polluted) condition.

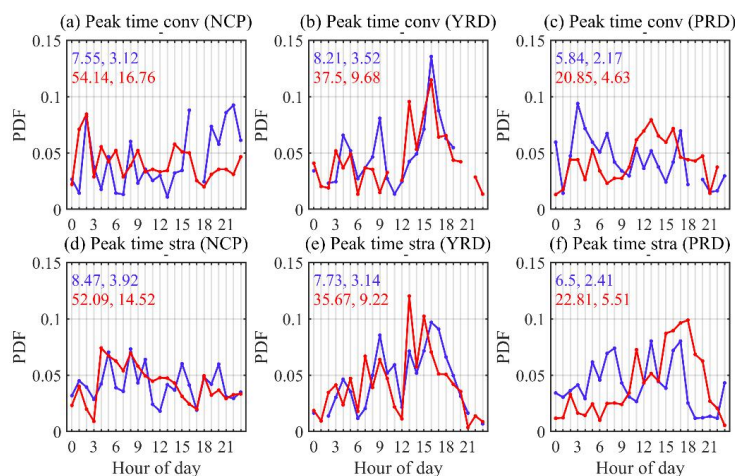
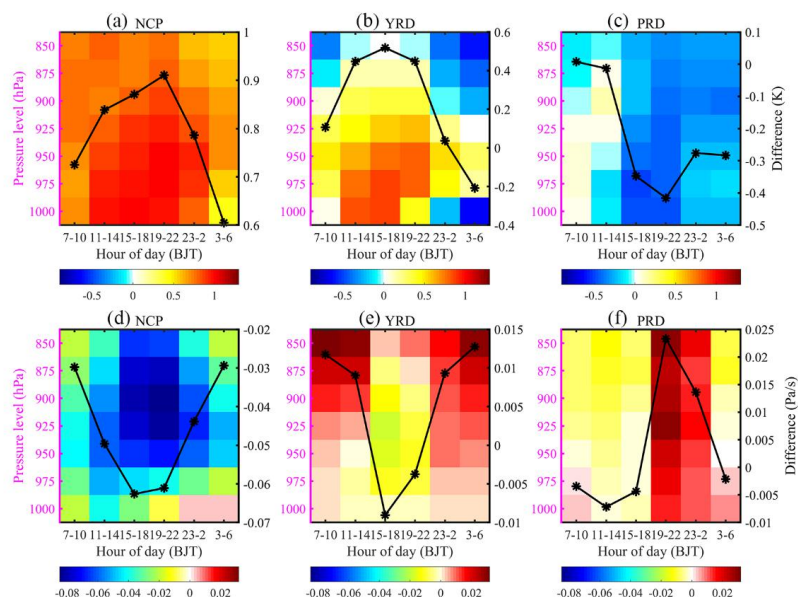
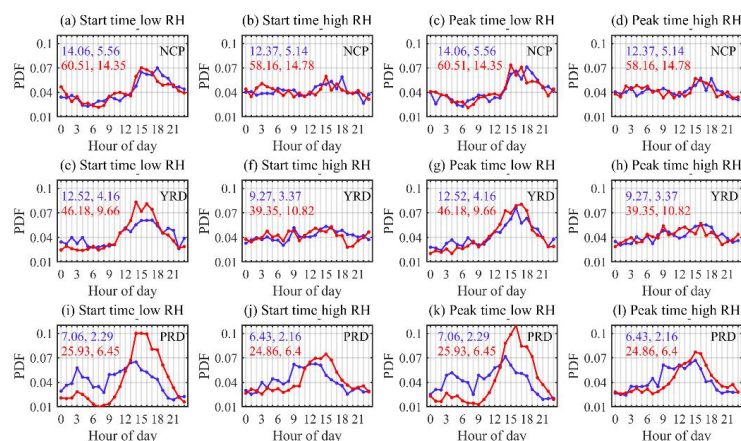


Figure 8: Same as Figure 7, but for (a-c) convective precipitation peak time and (d-e) stratiform precipitation peak time (units: LT).



875  
 876 Figure 9: The differences in (a-c) temperature (K) and (d-f) vertical velocity (Pa/s) between polluted  
 877 and clean conditions in NCP, YRD and PRD at different pressure levels. The positive (negative) values  
 878 represent heating (cooling) of the atmosphere in (a-c). The positive (negative) values represent down  
 879 (up) airflow in (d-f). The black lines represent the means of the differences in temperature (vertical  
 880 velocity) from 1000 to 850 hPa for several given hour periods, including 7:00-10:00, 11:00-14:00,  
 881 15:00-18:00, 19:00-22:00, 23:00-2:00 (the next day) and 3:00-6:00 LT.



882



Figure 10: Normalized PDFs of precipitation start time under (a, c, i) low humidity condition and (b, f, j) high humidity condition, the precipitation peak time under (c, g, k) low humidity condition and (d, h, l) high humidity condition in June–August from 2015 to 2020 over NCP, YRD and PRD, respectively. The blue (red) numbers are the average (the first column) and standard deviation (the second column) of the  $PM_{2.5}$  mass concentration ( $\mu g/m^3$ ) under clean (polluted) condition. The RH represents the relative humidity.

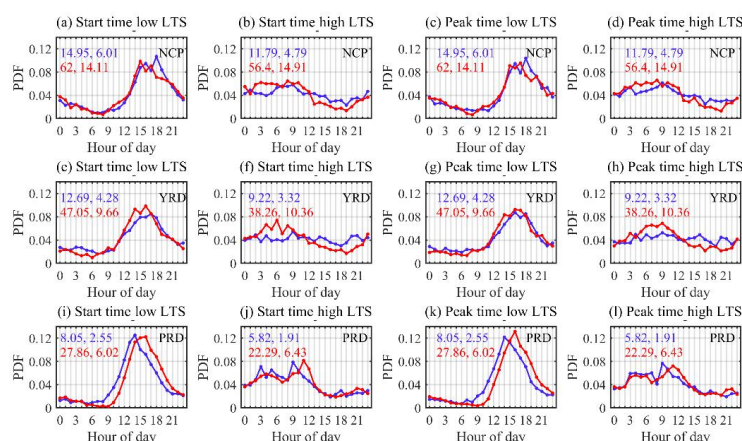


Figure 11: Same as Figure 10, but under low LTS condition and high LTS condition. The LTS represents low troposphere stability.

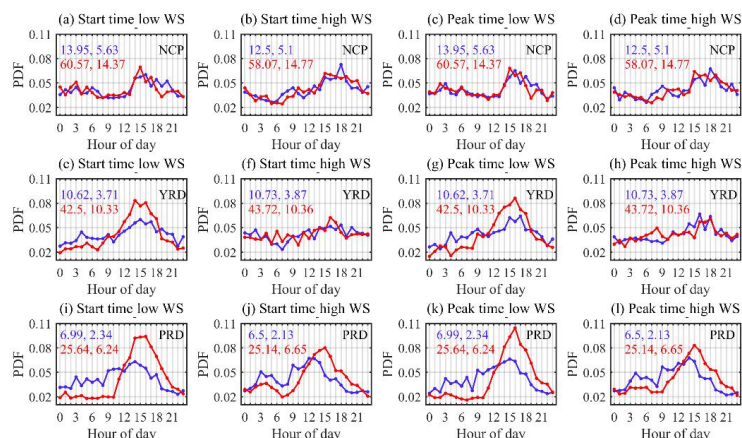


Figure 12: Same as Figure 10, but under low WS condition and high WS condition. The WS represents vertical wind shear between heights at 5500 m and 1500 m.